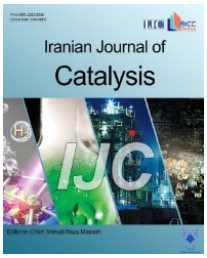

Iran. J. Catal. 2026; 16(1): 157-172

Iranian Journal of Catalysis (IJC)

https://doi.org/10.57647/ijc.2026.1601.10

Research Article

# The Effect of the Shapes of Zinc Oxide Nanoparticles on Antibacterial and Photocatalytic Activity via an Eco-Friendly Method

Hasti Samadi[1], Mehran Gholipour Shahraki [1,2,*], Reza Zarei Mohgadam[1,2*]

[1]*Department of Physics, Faculty of Science, Arak University, Arak, 384817758, Iran*
[2]*Institute of Nanoscience & Nanotechnology, Arak University, Arak, 384817758, Iran*

*Corresponding authors: r-zareimoghadam@araku.ac.ir, m-gholipour@araku.ac.ir

**Article History:**

Received:
29 October 2025

Revised:
10 December 2025

Accepted:
18 December 2025

Published Online:
24 December 2025

Published in Issue:
31 March 2026



**Abstract**

Mitigating the environmental risks associated with the chemical fabrication of nanoparticles is a pressing necessity. The green synthesis approach is considered a more secure alternative for nanoparticle production due to its cost efficiency, non-toxic nature, and eco-friendliness. Numerous elements influence the efficacy of nanoparticles; notably, the shape of these particles plays a crucial role, as their geometry can dictate their interactions with external factors, including biological organisms and water pollutants. For synthesizing Zinc oxide nanoparticles (ZnOn), Fig leaf extract was employed, which possesses antifungal, anti-helminthic, and acetylcholinesterase-inhibitory properties. For the first time in his work, he created different shapes of ZnOn with the same co-precipitation procedure and different calcination temperatures (200 °C, 400 °C, and 600 °C). To explore the impact of nanoparticle shape, a range of analytical methods has been utilized. The crystallite sizes of ZnOn were measured using the Debye-Scherrer method at forms of nanoflake, cylinder, and sphere, yielding 25.34 nm, 42.49 nm, and 43.52 nm, respectively. Moreover, UV-vis spectroscopy has identified a peak absorption wavelength of around 380, and characterizes the optical properties of ZnOn. Spherical nanoparticles exhibited the highest photocatalytic activity efficiency, reaching 88% in the first 60 min for ZnOn. The investigation focuses on the degradation process of methylene orange. Anti-microbial characteristics against the gram-negative (*E. coli*) and gram-positive (*S. aureus*) are examined by the MIC test for three samples of ZnOn.

**Keywords:** Anti-microbial activity; Fig leaf extract; Green synthesis; Photocatalytic activity; Zinc oxide nanoparticles

**Cite this article:** H. Samadi, M. Gholipour Shahraki, R. Zarei Mohgadam, Iran. J. Catal. **16** (2026) 157-172. https://doi.org/10.57647/ijc.2026.1601.10

## 1. Introduction

Recent evidence indicates that many scientists concentrate more on nanoscience than in previous years, largely due to this domain's exceptional physical and chemical characteristics. Chemical methods for generating nanoparticles have limited their broader applications due to the use of toxic chemicals. Additionally, catalytic applications may lead to adverse effects due to the accumulation of numerous hazardous compounds produced by chemical methods [1]. Ultimately, the advent of a groundbreaking approach known as green synthesis has effectively addressed numerous limitations, thereby paving the way for innovative strategies in the production of nanoparticles. Furthermore, the researcher's significant focus on synthesizing inorganic and organic nanoparticles

is owing to their extensive utilization in the biomedical field. The green method has been applied to a diverse array of biological materials for the synthesis of nanoparticles. Bioactive molecules are identified within the biological extracts derived from various sources, including plants, algae, bacteria, and viruses. Biomolecules are vital in reducing and capping, leading to decreased metal toxicity and enhanced biocompatibility. Green nanoparticles are not only cost-effective and environmentally sustainable, but they also eliminate the necessity for stabilizers. The surfaces of green nanoparticles exhibit a propensity to adsorb biomolecules when they come into contact with cellular fluids, resulting in the formation of a corona that offers an additional benefit [2]. The combination of marine resources and extracts from medicinal plants significantly enhances the pharmacological attributes of green nanoparticles, thereby increasing their potential applications in biomedical and related disciplines [3].

Recently, semiconducting metal oxide nanoparticles have gained significant attention as catalysts for treating water and wastewater containing organic pollutants [4]. Their unique properties, such as a tunable band gap, high surface area, and the ability to generate reactive oxygen species (ROS), enable them to perform various functions, including antibacterial, antioxidant, and anticancer activities [5], as well as applications in photocatalysis [6] and the textile industry [7].Zinc oxide is an inorganic semiconductor with remarkable attributes, including substantial binding energy, an extensive band gap, and significant piezoelectric properties [8]. This exhibits three distinct crystalline forms: wurtzite, rock salt, and Zinc blend. Under standard environmental conditions, the wurtzite structure exhibits thermodynamic stability, characterized by each Zinc atom being tetrahedrally coordinated to four oxygen atoms [9]. Furthermore, Zinc oxide nanoparticles (ZnOn) are characterized by their non-toxic nature [10], self-cleaning properties, and skin-friendly attributes [11]. Numerous factors, such as dimensions, form, stability, and others, significantly influence the potential applications of nanoparticles [12, 13]. In this context, the morphology of nanostructures holds significant importance as it directly influences their photocatalytic and antibacterial characteristics. Various types of nanostructures (such as spheres, cubes, wires, plates, etc.) exhibit distinct behaviors due to variations in specific surface area, crystal surface energy, or light absorption[13, 14].

The influence of shape on photocatalytic characteristics can be related to the variations in surfaces, because larger surfaces facilitate enhanced absorption and promote the separation of electron-hole pairs, thereby improving efficiency[15, 16]. Furthermore, nanoparticles characterized by sharp edges facilitate more intimate contact and increased disruption of the bacterial cell membrane. In contrast, spherical nanoparticles exhibit a milder interaction with the cell, which accounts for their application in medical fields, particularly in drug delivery[17, 18].

Considering the various biological characteristics of *Ficus carica* leaves and the existence of biomolecules contained within them, this extract was utilized for the environmentally friendly synthesis of ZnOn. These isolated bioactive compounds (such as flavonoids and tannins) demonstrate a wide range of health-enhancing properties. The various components of *Ficus carica*, including its leaves, roots, fruit, and latex, are recognized for their significant biological and health benefits. The properties related to *Ficus carica* leaves are mentioned below. Nutrients in fig leaves include[19]:

- Fiber: Comprises a substantial quantity of dietary fiber, which aids in the process of digestion.
- Vitamins: Fig leaves provide a beneficial source of vitamins, including vitamin A, vitamin C, and vitamin E.
- Minerals: Fig leaves are a source of vital minerals such as calcium, magnesium, potassium, and iron.
- In addition, fig leaves have many health and medical benefits, including the following [20]:
- Lower blood pressure: Fig leaves contain a high concentration of potassium, which plays a crucial role in managing elevated blood pressure by counteracting the detrimental effects of sodium within the body [21].
- Heart health: The antioxidants found in fig leaves serve to safeguard the heart against damage caused by free radicals, leading to enhanced cardiovascular health and a reduced likelihood of heart disease [22].
- Anti-diabetic activity: Fig leaves have demonstrated the ability to lower blood sugar levels, thereby assisting in the management of diabetes symptoms[23].
- Weight management: Rich in dietary fiber, fig leaves may assist in appetite regulation and contribute positively to weight loss efforts[24].
- Bon health: Fig leaves are a source of calcium, a vital nutrient necessary for the maintenance of robust and healthy bones, as well as for enhancing bone density [25].
- Boosts immunity: Fig leaves are abundant in vitamins A, B1, and B2, which have the potential to enhance the immune system [26].
- Anti-bacterial activity: Fig leaves possess antibacterial characteristics that can safeguard against prevalent bacterial infections [27].

Methylene orange is used in this study as a probe to examine the photocatalytic effect, which is extensively used in the cotton industry. The exceptional quantum efficiency of ZnOn has led to its extensive application as

10.57647/ijc.2026.1601.10

a prominent photocatalyst for organic dyes [6]. This research, for the first time, examines the alteration in shape of nano material (ZnOn) due to varying calcination temperatures, and explores the influence of nanoparticle shape on characterization, photocatalytic, and antibacterial properties. Furthermore, it demonstrates that changes in the shape of a nanoparticle can considerably impact its properties. Previous studies have investigated the dimensions of various nanoparticle shapes utilizing diverse synthesis techniques such as chemical methods, green synthesis, and others or employing different precursor materials [28, 29].

This underscores the significance of this research. Consequently, the materials and synthesis techniques of the nanoparticles have been detailed for this purpose. XRD analysis was employed to assess the crystallinity of the structure. UV-Vis analysis was utilized to evaluate the optical properties, while FT-IR analysis was conducted to investigate the bonds.

The morphology of the nanoparticles was analyzed using FESEM. The photocatalytic and antibacterial properties of them with varying shapes were examined, aligning with findings from another research.

## 2. Experimental details

### 2.1. Materials and methods

The materials used in this investigation included Zinc nitrate hexahydrate ($Zn(NO_3)_2.6H_2O$) with a purity level of 99.9% and sodium hydroxide (NaOH) at 99% purity from the Merck brand, alongside deionized water, which was applied at all experiment stages.

### 2.2. *Ficus carica* (fig) leaf extraction procedure

The fig leaves were collected from a garden situated in Karaj, Iran. The leaves underwent multiple washings with tap water, followed by a rinse with deionized water to eliminate any surface contaminants. Then, the leaves were cut and placed in direct sunlight to achieve complete desiccation. After that, the dried leaves are crushed extensively and sieved twice to ensure uniformity. The final step involves grinding the material until a soft powder is obtained. To extract *Ficus carica* (fig) leaves, 20 g of leaf powder was mixed with 800 mL of distilled water. The aqueous mixture was heated to a boiling point until its color transitioned to a light yellow, which generally takes around 20 min to achieve. Following this, when the mixture has cooled to ambient temperature, it is necessary to filter it through filter paper, Whatman Number 1. Utilizing a rotary pump will facilitate a more rapid passage through the filter. To eliminate the biomaterials, the solution underwent centrifugation at 2000 rpm for 10 minutes. For subsequent synthesis, it is essential to store the extract in the refrigerator at 4 °C.

### 2.3. Nanoparticle fabrication

44.62 g of Zinc nitrate hexahydrate ($Zn(NO_3)_2.6H_2O$) was dissolved in 300 Ml of double-distilled water, which served as the solvent. Subsequently, 6 ml of a light-yellow extract was added to the solution, and the mixture was stirred for 10 min to ensure homogeneity. Incrementally add NaOH (2 M) to the solution, noting that the color shifts from pale yellow to white until the Ph level reaches 11. The powder was dried at 90 °C for 5 hours. The final step for creating the various ‘shapes’ of ZnOn related to calcination temperatures at 200 °C, 400 °C, and 600 °C for 2 hours. It's happened due to the influence of biomolecules on the size and morphology of ZnOn. For the first time, we create different ‘shapes’ of ZnOn with the same co-precipitation method by changing the calcination temperatures, according to the relation.

$$Zn(NO_3)_{2(aq)} + 2Na \rightarrow Zn(OH_{2(S)}) + 2NaNO_{3\ (aq)}$$
$$\rightarrow Zn(OH_2)(s) \rightarrow^{\Delta} ZnO(s) + H_2O(g)$$

## 3. Results and discussion

### 3.1. Strategies for Characterization

This study investigates the morphological, optical, and structural characteristics of zinc oxide nanoparticles (ZnOn) synthesized under three distinct shapes. Structural analysis was performed utilizing X-ray diffraction (XRD) with CuKα radiation (λ = 1.54060 Å) within a 2θ range of 10° to 85°, employing a step size of 0.05°. This allowed for a detailed assessment of crystalline structure and phase identification. Furthermore, field emission scanning electron microscopy (FESEM) was employed to evaluate the surface morphology and particle size distribution of the ZnOn samples.

The Data alignment from XRD and FESEM provides a comprehensive understanding of the relationship between the nanoparticle’s form and the resulting structural and morphological properties of the ZnOn. Figure 1 presents a comprehensive schematic detailing the entire process from initial material extraction to final nanoparticle synthesis.

This visual representation clarifies the distinct stages involved, outlining reagent usage, reaction conditions, and purification techniques. Crucially, the figure also illustrates the analytical methodologies employed to characterize the synthesized nanoparticles, including techniques used to determine size, morphology, composition, and crystalline structure, ensuring a thorough understanding of the material's properties.

10.57647/ijc.2026.1601.10

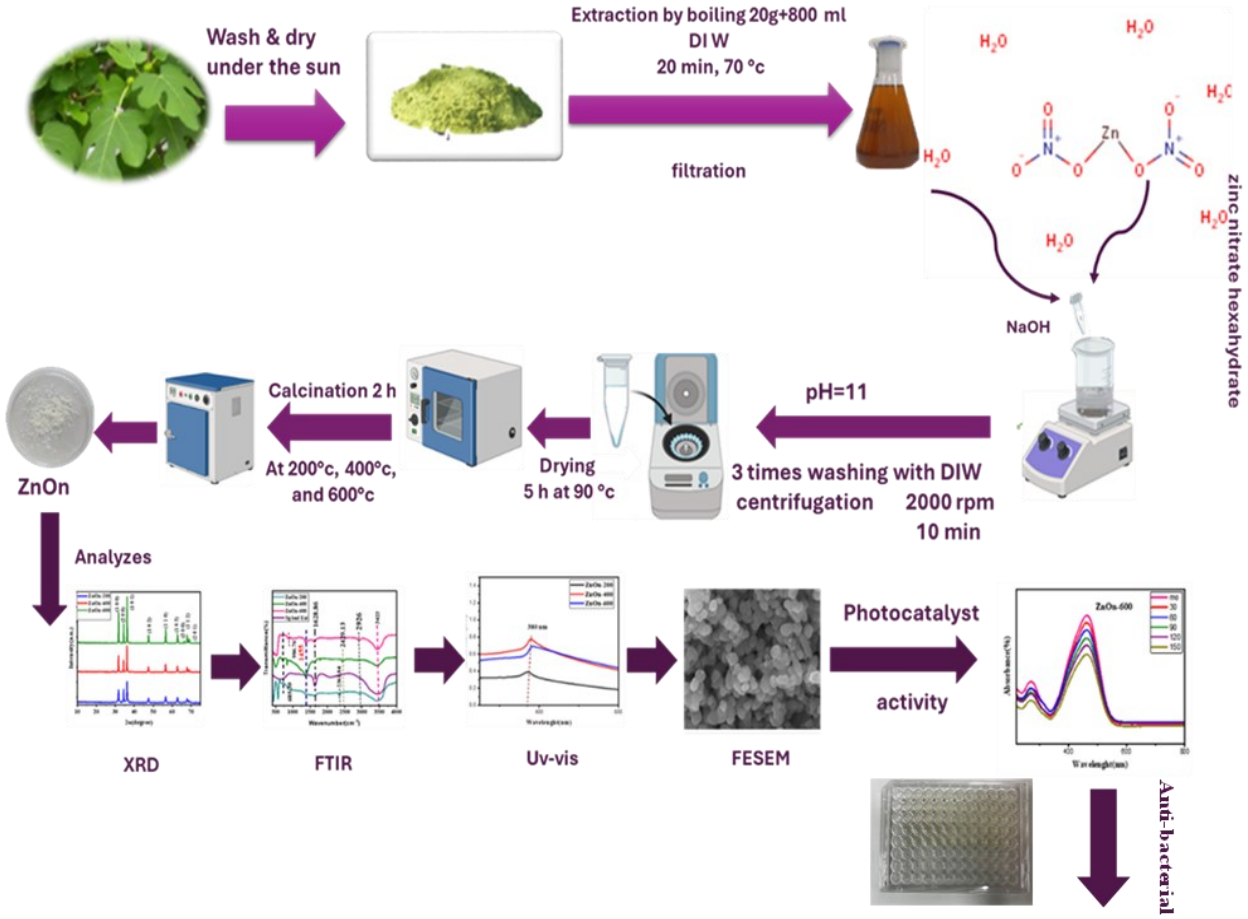


**Figure 1**. Schematic diagram for the synthesis of ZnOn

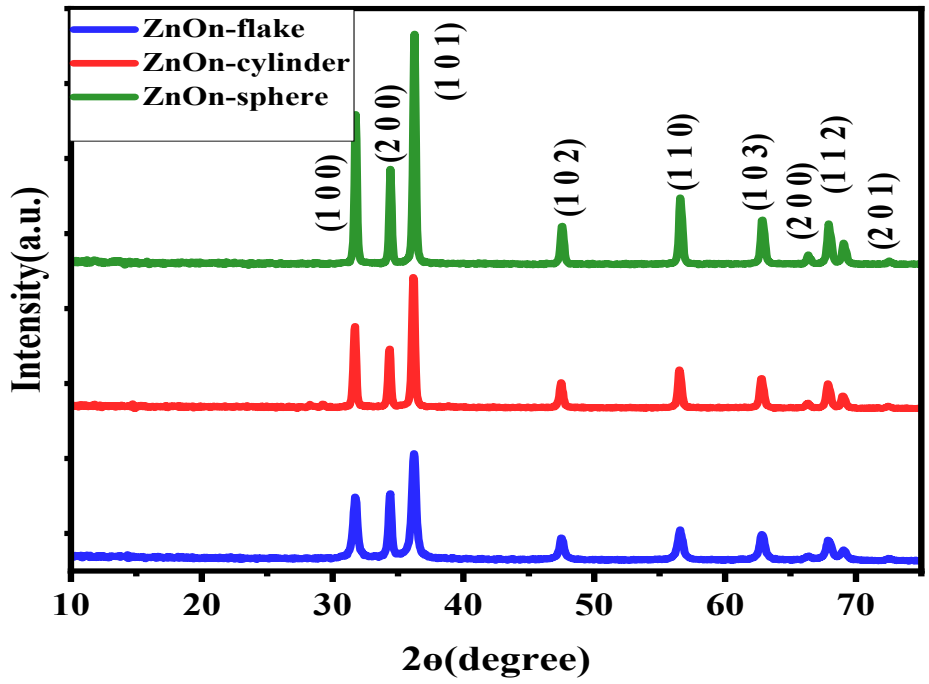


**Figure 2**. pattern of XRD related to ZnOn in various shapes synthesized via fig leaf extract

3.1.1. *X-ray diffraction analysis*

Figure 2 illustrates the XRD patterns obtained from ZnOn that were generated at three separate forms of nanoflake, cylinder, and sphere. Peaks associated with ZnOn were detected in three samples; they exhibit complete compatibility with the JCPDS standard card (No. 01-089-7102).

Various distinct peaks have been identified at the following angles:2ɵ= 81.397°, 76.955°, 69.032°, 67.873°,

10.57647/ijc.2026.1601.10

66.314°, 63.809°, 56.545°, 53.872°, 47.515°, 39.222°, 35.31°, and 34.36° corresponding to (1 0 0), (2 0 0), (1 0 1), (1 0 2), (1 1 0), (1 0 3), (2 0 0), (1 1 2), and (2 0 1). An elevation in calcination temperature results in an enhancement of crystallinity.

Further investigations conducted by other scholars have substantiated this conclusion [7]. The crystallite size of ZnOn, defined by its (h k l) orientations, can be estimated using Scherrer's formula (equation 1) [30].

$$D = \frac{K\lambda}{\beta \cos\theta} \quad (1)$$

In this context, the wavelength of the employed radiation is denoted as λ, the Bragg angle is represented by θ, and the shape factor is defined as K = 0.9. β represents the full width at half maximum (FWHM) of the X-ray diffraction (XRD) peak [31].

The nano-crystallite sizes of ZnOn-sphere, ZnOn-cylinder, and ZnOn-flake are determined to be 43.53 nm, 42.49 nm, and 25.34 nm, respectively. The alteration in calcination temperature led to the deformation of the nanoparticles, which did not significantly impact their crystallinity, as evidenced by XRD analysis[32]. Furthermore, the purity of the nanoparticles was demonstrated in three distinct forms.

Additionally, the deformation of the nanoparticles influenced their crystallite size, with sharper nanoparticles exhibiting smaller crystallite sizes compared to those with smoother shapes [33].

Similarly, the green synthesis of ZnOn has been successfully carried out using different natural substances, such as *Ficus benghalensis* extracts [34], *Mulberry* Fruit [35], *Myrtus communis* plant extract [36], *Citrus sinensis* extract [37].

### 3.1.2. *FT-IR analysis*

FTIR analysis is known for its ability to identify functional groups. Changes in morphology cause variations in peak intensity, shifts, and bandwidths. As a result, increasing the specific surface area of nanoparticles correlates with higher peak intensity. Furthermore, morphological changes affect peak shifts due to modifications in the chemical environment around functional groups.

Additionally, nanoparticles with irregular shapes or surface imperfections show broader bandwidths [35]. Figure 3 presents the FTIR spectrum features associated with the functional groups of ZnOn, with a wavelength range from 400 to 4,000 $cm^{-1}$[36].

The absorption band near 11455 cm-1 indicates a strong vibrational bond between Zinc and Oxygen [37]. In addition, the nanoparticles show absorption peaks at 1630 $cm^{-1}$ and 3422 $cm^{-1}$, indicating O-H bonds and their vibrational modes [38]. The fig leaf extract displayed peaks at 3448 $cm^{-1}$ and 1636.22 $cm^{-1}$, signaling strong O-H bonds and weaker C-H bonds linked to aromatic compounds. These peaks, with slight shifts across three nanoparticle samples, suggest the presence of extract bonds within the nanoparticles.

The spectral range of 2926 cm-1 relates to the C-H bonds typical of alkanes [39], while bands at 1628 $cm^{-1}$ reflect the stretching modes of carbon-carbon (C-C) bonds. The spectrum from 720 $cm^{-1}$ to 986 $cm^{-1}$ shows the stretching vibrations of aromatic C-H bonds [40].

The observed bands are associated with biomolecules in the fig leaf extract, such as polyols, flavonoids, and proteins, which play a key role in the bioreduction and stabilization of ZnOn, as noted in previous studies [5].

The results suggest that changes in nanoparticle morphology influence peak intensity. As the surface asymmetry of nanoparticles increases, there is a corresponding rise in peak intensity and shift. Polar functional groups, including (–OH, –COOH, $–NH_2$, C=O), induce the most significant alterations in FTIR [38].

In this research, cylindrical nanoparticles, the most asymmetric configuration, exhibit higher peak intensity and a greater shift. In addition, a slight shift was observed in the peaks. Similar findings have been reported by Shen, Lazhen, et al [39, 41].

### 3.1.3. *Ultraviolet-visible spectroscopy*

Figure 4 indicates the UV-Vis spectra of ZnOn at various shapes. The absorption peak of ZnOn is displayed around 370 nm [40] .

The absorption peak of green nanoparticles of ZnO at different shapes is obtained around 385 nm. The findings indicate that variations in the morphology do not influence absorbance.

The movement process of an electron transitioning from the valence band to the conduction band introduces an absorption peak. In addition, the band gap energy of a semiconductor is influenced by size and morphology [41]. Therefore, according to the values obtained from XRD analysis, the size of the nanoparticles increased with increasing calcination temperature. It's proven by the other study [33, 42]. Consequently, with increasing size, diminishing surface particle, the band gap of the nanoparticles decreased so that using the Tauc relationship, the band gaps of ZnOn-flake, ZnOn-cylinder, and ZnOn-sphere were 2.1, 1.6, and 1.38, respectively.

Similar findings have been observed in related research [43]. The band gap is calculated using Tauc's equation (Figure 4)[44]. The Tauc's equation is derived from the subsequent relationship, which is shown in equation (2)[45].

$$(\alpha h\nu)^2 = k(h\nu - E_g) \quad (2)$$

10.57647/ijc.2026.1601.10

Here, the symbol α denotes the extinction coefficient, $E_g$ The energy gap, the constant (k), exhibits varying values depending on the specific transitions involved; hv is the energy of a photon .The measured band gaps for the samples. Furthermore, it demonstrates that the shape of nanoparticles is adapted to the band gap [46].

3.1.4. *FESEM analysis*

Figure 5 indicates the surface structure of ZnOn samples. Micrographs indicate a significant degree of agglomeration among ZnOn, which exhibits a particle-like morphology characterized by irregular shapes.

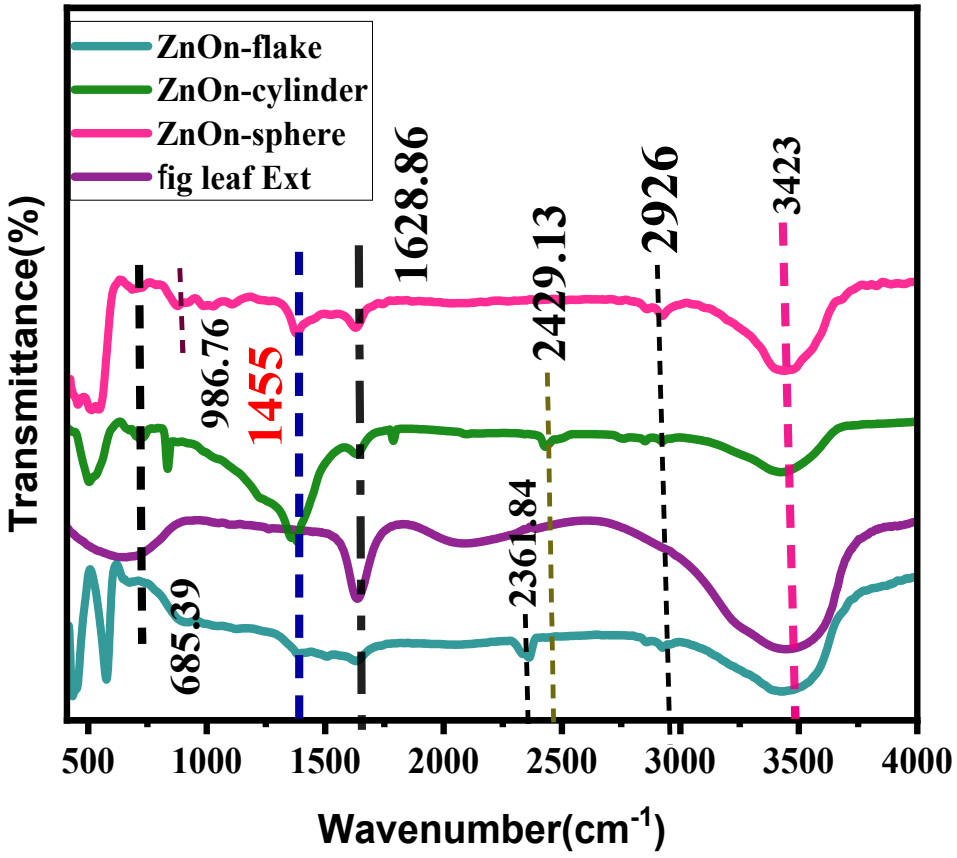


**Figure 3**. The FTIR spectrum is related to ZnOn via fig leaf extract at three types of shapes

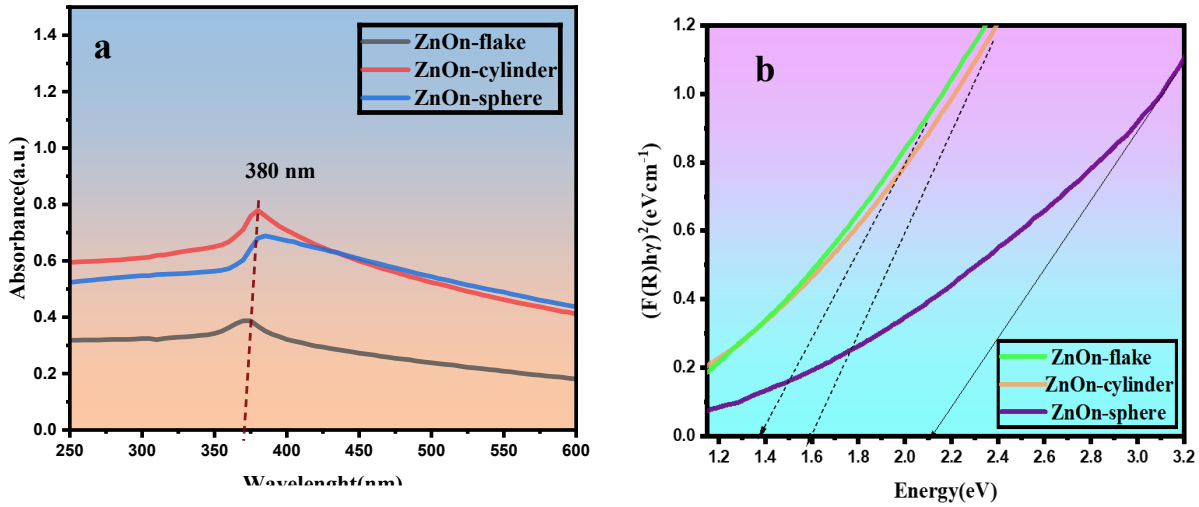


**Figure 4**. a) The UV-Vis spectra of ZnOn and b) the calculated band gap of ZnOn at various shapes

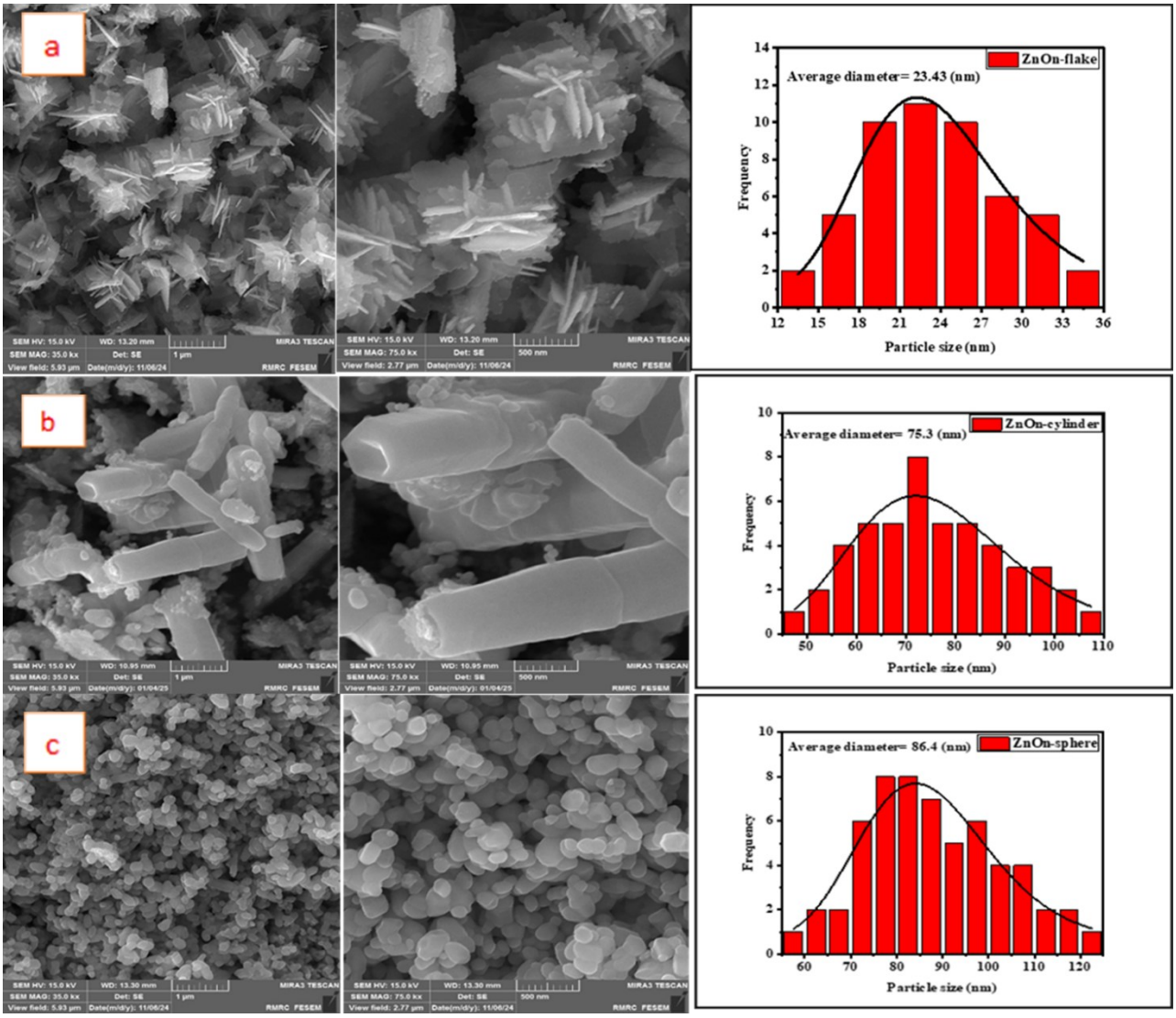


**Figure 5**. FESEM images of ZnOn synthesized by fig leaf extraction at (a)flake, (b)cylinder, and (c) sphere

This observation aligns with the findings of Sedefoglu [47], who discussed the synthesis of ZnO nanostructures through a green synthesis method. The significant surface energies associated with ZnOn result from the clustering of nanomaterials or the formation of larger nanoparticle entities [48]. The calcination of ZnOn at a temperature of 200 °C results in a nanoflake architecture (ZnOn-flake) that appears almost regular in form. Modifications to the temperature during the calcination process result in changes to the morphological characteristics [47]. Observations indicate that ZnOn exhibits a hexagonal cylindrical morphology at a temperature of 400 °C (ZnOn-cylinder). The shape of ZnOn has been observed to be spherical at 600 °C (ZnOn-sphere). The average diameter of nanoparticles is estimated using the log-normal distribution equations (3-5).

$$f(D) = \left(\frac{1}{\sqrt{2\Pi}\delta D}\right) exp\left[\frac{ln^2\left(\frac{D}{D_0}\right)}{2\delta^2}\right] \quad (3)$$

$$\langle D\rangle = D_0\, exp\left(\frac{\delta^2}{2}\right) \quad (4)$$

$$\delta_D = \langle D\rangle[exp(\delta^2 - 1)]^{\frac{1}{2}} \quad (5)$$

The parameters Dand $\delta_0$ were derived from equations 3-5. Furthermore, these equations were employed to calibrate the data. As the shape changed from flask to sphere, the average diameter of the nanoparticles was 23.43,75.3, and 86.4 nm, respectively. These results are consistent with the particle size identified through X-ray diffraction (XRD) analysis. The reason for that is that at lower temperatures, the influence of biomolecules on the morphology of nanoparticles with a greater surface area becomes more pronounced. Consequently, with rising temperatures, the nanoparticles undergo growth and increased aggregation, resulting in alterations to their shape [49]. This research introduces an innovative approach that leverages the characteristics of biomolecules by varying the calcination temperature to obtain diverse morphologies suitable for medical or photocatalytic applications. This occurrence has also been reported in several other research studies [50-52].

10.57647/ijc.2026.1601.10

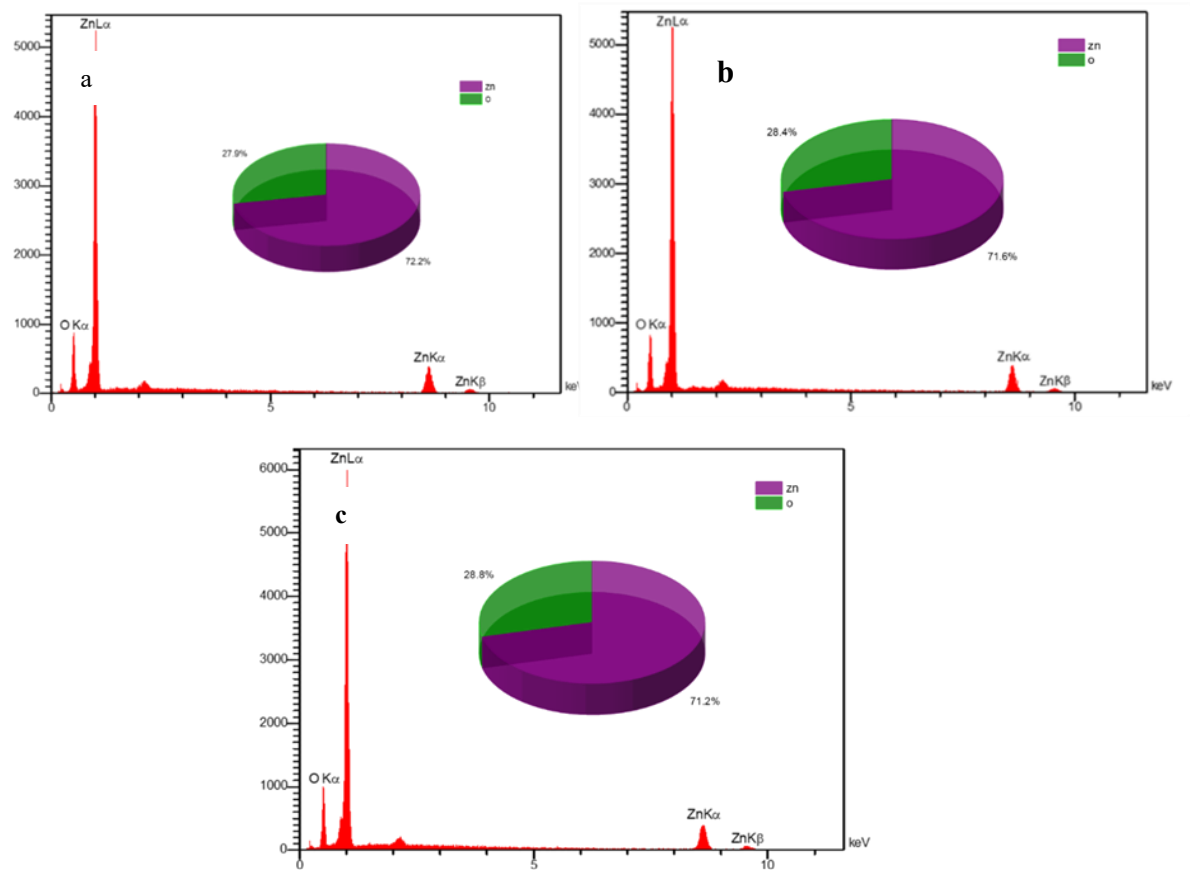


**Figure 6**. EDS analysis for ZnOn generated by fig leaf extract. a) ZnOn-flake, b) ZnOn-cylinder, and c) ZnOn-sphere

3.1.5. *EDS analysis*

EDS analysis determines the material's elemental constituents. Figure 6a-c present the EDX spectra of green-synthesized samples at three different nano shapes. In this study, the purity percentages of Zinc (Zn) and Oxygen (O) were assessed as follows. For the sample designated ZnOn-flake, the concentrations were determined to be 72.15% for Zn and 27.85% for O. For the ZnOn-cylinder sample, these values changed to 71.55% for Zn and 28.45% for O. Furthermore, ZnOn that have a spherical shape showed purity percentages of 71.18% for Zn and 28.82% for O. The fact that Zn and O both have peaks that are matched in size means that the purity of the ZnOn in all three forms has been confirmed, while the near identical percentages of the two peaks show that the morphology of the Nano particles does not influence the amount of surface elements present. Many researchers have confirmed the same findings in their own studies [53]. In addition, Figure 6 shows EDS spectra for various forms. A lot of research has been conducted on the green synthesis of ZnOn, and a few notable examples can be mentioned. Irshad, Muhammad Atif, et al. used Ficus benghalensis extracts to generate ZnOn. They used different analyses, such as EDS, to analyze the nanoparticles of zinc oxide and confirm their presence [34].

## 3.2. Photocatalytic activity of ZnOn

In recent decades, nanoscale metal oxide semiconductors have been developed for use as catalytic materials, demonstrating significant potential in solar water purification. The efficacy of transition or d-block metal ions in extensively researched semiconductors has been notable, positioning them as highly effective components in the creation of photocatalytic materials [54]. Various elements play a significant role in enhancing the photocatalytic process, such as the Dye solution concentration, the Quantity of catalyst, the pH, and the structural characteristics of the photocatalyst's surface [55]. Furthermore, numerous research efforts have enhanced the performance of photocatalysts through re-engineering; for instance, a method to transform a heterogeneous type-11 photocatalyst into a perovskite-based Z-design has demonstrated increased efficiency of a perovskite-based photocatalytic system for CO2 reduction [56]. Additionally, a separate study carried out in 2025 revealed that the incorporation of trace amounts of Zn and Al either as impurities or through doping significantly improved the catalytic activity of $Nb_2O_5$ in hydrogen evolution reactions (HER)[57]. Another study illustrates the effects and benefits of defect (oxygen vacancy) engineering in $TiO_2$-based photoelectrodes, showing that this heterogeneous configuration provides

10.57647/ijc.2026.1601.10

enhanced performance relative to reference systems (e.g., defect-free $TiO_2$ or simpler heterogeneous structures). $TiO_2$-x-$MoS_2$ electrodes exhibit a 13-fold enhancement in photoelectrochemical activity when compared to unmodified $TiO_2$ nanorods and demonstrate a low overpotential. This improvement is attributed to the accelerated electron transfer kinetics at their interface, a decrease in the charge recombination rate, an increase in charge carrier density, and a highly wettable surface [58, 59]. The other paper reports that strontium Sr-doped in ZnOn leads to modifying particle morphology and influencing photocatalytic dye degradation[60]. In other studies, the best photodegradation activity for the drug Sulfasalazine with ZnO–NiO was observed at pH ≈ 6.5, close to the pH_pzc (point of zero surface charge) of the composite [61]. Extract is another factor that influences photocatalyst activity due to compounds such as flavonoids, tannins, polyphenolics, and –OH groups, suggesting they would modify particle size, shape, and defect on the surface of the particle. As a result, alterations occur that increase production of reactive oxygen species (ROS), which contribute to the photocatalysis. Several other studies have examined this area [62].

In this article, the role of the extract and temperature is also explained in the section related to FESEM analysis. Conversely, the photocatalytic performance of nanoparticles is influenced by their shape and size, which can impact the separation and recombination of electron-hole pairs[63]. Furthermore, the other study demonstrates that the shape of the nanoparticle is sensitive to its size; so the sharp crystals possess much higher activity than the flat crystals in the oxygen evolution reaction, which, in combination, leads to the morphology dependence of photocatalytic activity [64, 65]. Therefore, modifying the structure and morphology of nanoparticles (through nanocomposites and doping) can enhance photocatalytic efficiency. This has been demonstrated in previous studies [66, 67].

This study focuses on the breakdown of organic waste and cleansing environmental contaminants. In Figure 7, the absorption spectra related to the degradation of methyl orange (MO) under Xenon radiation, employing the samples of ZnOn as a photocatalyst, are displayed. The study investigates the photocatalytic activity and photodegradation of ZnOn samples for degrading (MO) dye when subjected to 50 W xenon lamp radiation, as illustrated in Figure 8(a). (ZnOn) are applied as a single-material photocatalysis. To prepare a (MO) solution at a concentration of 15 ppm, dissolve 0.0015 g of the dye in 100 mL of deionized water. Following this, incorporate 0.0036 g of ZnOn-sphere into 50 mL of (MO) and maintain stirring for 30 minutes in a dark environment to optimize its effectiveness. An identical procedure was conducted for the ZnOn-flake and ZnOn-cylinder.

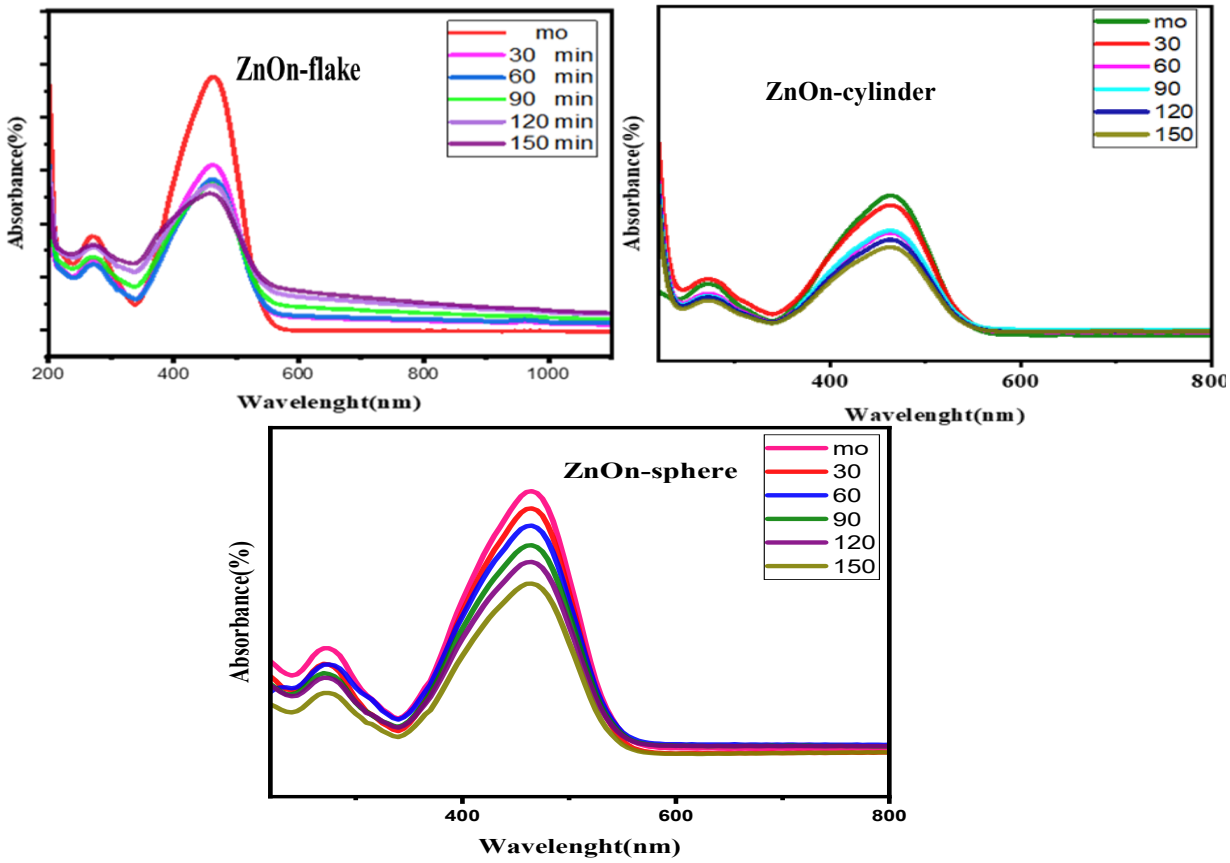


**Figure 7**. Photocatalytic activities of ZnOn utilizing fig leaf extraction for ZnOn-flake, ZnOn-cylinder, and ZnOn-sphere samples

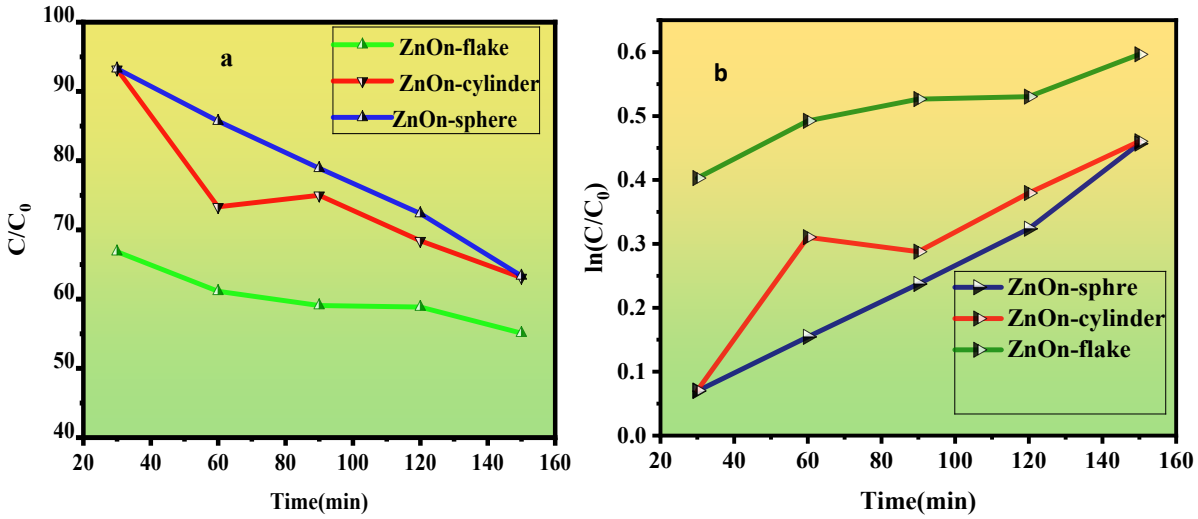


**Figure 8**. (a) The percentage of degradation for ZnOn in different forms. (b) plot of ln($^{C}/_{C_0}$) related to three sa

The analysis revealed that ZnOn-flake exhibits a greater ability to degrade color than the other two ZnOn types. This enhanced performance may be linked to their crystal structure and the larger surface area presented by the nanoflakes, as presented in Figure 5.

The plot related to the percentage of degradation for three samples of ZnOn is depicted in Figure 8 a. One can ascertain the efficiency of degradation by employing equation 6.

$$\eta = \frac{C-C_0}{C_0} \times 100 \quad (6)$$

Where $C_0$ represents the initial concentration, while $C$ indicates the concentration at a particular time [68]. Figure 8b illustrates the relationship between $\ln(c_0/c)$ and irradiation time for all samples analyzed. Furthermore, the graph of $\ln(C_t / C_0)$ against irradiation time investigates the kinetics of the photocatalytic reaction, as illustrated in Figure 8b for three samples, ZnOn. The linear relationship can be expressed through the following equation (7) [69, 70].

$$\ln\left(\frac{C_t}{C_0}\right) = ln\left(\frac{A_t}{A_0}\right) = Kt \quad (7)$$

$C_o$ and $C$ present the initial absorbance of the dye before degradation and the absorbance of the dye at time "t" after degradation, respectively. The slope of this linear equation is represented by k and was used to calculate the homogeneous constant. The decolorization efficiencies of ZnOn in nano flake, cylinder, and spherical shapes are recorded as 63.83%, 63.1%, and 53.39%, respectively. As previously stated, this was also demonstrated in the current study. The more defined surface of the nanoparticles facilitated the oxygen evolution reaction and enhanced the photocatalytic activity [64]. In the photocatalytic degradation process, the absorption wavelength decreases noticeably, corresponding to an increase in the illumination level [71]. The mechanism underlying photocatalytic activity is succinctly outlined as follows. ZnOn exposed to radiation from a xenon lamp results in the free electrons being excited. The excitation process generates pairs of electrons and holes, with the holes in the valence band and the electrons occupying the conduction band. The generation of OH radicals occurs through the secondary interaction between positive holes and electrons, leading to the breakdown of organic pollutants [72, 73]. Figure 9 illustrates the mechanism of ZnOn photocatalytic activity. Additionally, Table 1 compares different study results related to the photocatalyst activity of ZnOn.

### 3.3. Anti-bacterial test

The antibacterial mechanism of ZnOn can be explained by two primary mechanisms: 1. The generation of reactive oxygen species (ROS), 2. The interaction between nanoparticles and bacteria leads to damage to the bacterial cell wall and the release of $Zn^{+2}$ [81]. Numerous research studies have unequivocally demonstrated that water-soluble ZnOn are capable of generating a range of reactive oxygen species (ROS), such as hydroxyl radicals (•OH), superoxide anion ($O_2^{\bullet-}$), and hydrogen peroxide ($H_2O_2$)[82, 83]. The responses of ZnOn to bacterial agents are illustrated in equations 12-16[84].

$$ZnO + h\gamma \rightarrow e^- + h^+ \quad (12)$$

$$h^+ + H_2O \rightarrow \cdot OH + H^+ \quad (13)$$

$$e^- + O_2 \rightarrow \cdot O_2^- \quad (14)$$

$$\cdot O_2 + H^+ \rightarrow HO_2 \quad (15)$$

$$HO_2 + H^+ + e^- \rightarrow H_2O_2 \quad (16)$$

Conversely, functional groups like (OH, –COOH, –NH2, C=O-) play a crucial role in the interaction between nanoparticles and the bacterial cell wall [85]. Studies have demonstrated that altering the configuration of

10.57647/ijc.2026.1601.10

nanoparticles can enhance bacterial activity. The efficacy of doped ZnOn in addressing bacterial infections and enhancing hygiene across multiple domains [60, 86]. Moreover, enhancing the surface area of nanoparticles results in a rise in reactive oxygen species (ROS) production, a phenomenon documented in numerous studies [83, 87]. The morphology and functional group of ZnOn (from FT-IR analysis) whether flake, cylinder, or sphere coupled with their diminutive size, contribute to an increase in surface area, changing in the functional group on the surface, thereby augmenting their antibacterial properties. Conversely, nanoparticles exhibiting a more irregular shape demonstrate superior penetration capabilities into the bacterial cell wall. As demonstrated by Alshraiedeh, Nid'A. H., et al. in 2022, the destructive efficacy of flake nanoparticles surpasses that of spherical nanoparticles [88]. This study used Escherichia coli strain ATCC 25922 and S. aureus ATCC 25923 to examine their properties. The minimum inhibitory concentration (MIC) was determined by broth microdilution in 96-well microplates (Figure 10).

$$ZnOn + h\nu \rightarrow e_{CB}^{-} + h_{VB}^{+} \quad (8)$$

$$O_2 + e_{CB}^{-} \rightarrow .O_2^{-} \quad (9)$$

$$h_{VB}^{+} + H_2O \rightarrow OH \cdot \quad (10)$$

$$.OH + Methyle\ orange \rightarrow degradation \quad (11)$$

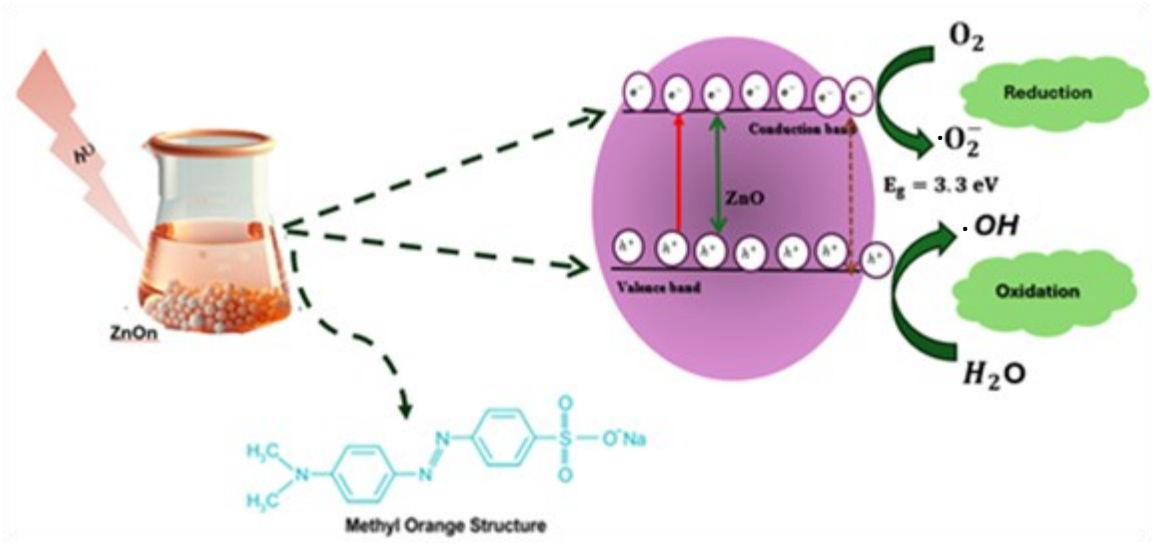


**Figure 9**. Mechanism of ZnOn photocatalytic activity

**Table 1.** The efficacy of Zinc oxide nanoparticles' photocatalytic activity using different extracts, compared to the results of this study over the first 60 minutes of the process

| Method | Botanical extract | Organic pollutant | Nanoparticle shapes | Light source | Duration of process (min) | Efficiency (%) | Ref. |
|---|---|---|---|---|---|---|---|
| Green | *Amomum longiligulare* | Methylene green | Semi spherical | UV | 60 | 38 | [74] |
| Green | *Corymbia citriodora leaf* | Methylene blue | ------- | Visible light | 60 | About 50 | [75] |
| Green | Garcinia xanthochymus | Methylene blue | spongy cave | UV-various pH<br>UV-various masses of ZnOn | 60<br>60 | About 45<br>About 45 | [76] |
| Green | Leaf Alchornea laxifora | Congo red | quasi-hexagonal | UV | 60 | 87 | [77] |
| Precipitation<br>Sol-gel | ----- | degrading phenol | Spherical Nanorod | UVA | 60 | 30<br>50 | [78] |
| Chemical | ------ | Methyl Orange | Spherical | UV-Vis | 60 | 47 | [79] |
| Green | Equisetum diffusum D | Methyl Orange<br>Methyl Blue | spherical | Sun light | 60<br>60 | 72.63<br>70 | [69] |
| Green | Wild olive leaves | Formic acid-Sodium formate | Spherical and hexagonal | UV | ------ | 80 | [80] |
| Green | Fig leaf extraction | Methylene orange | flake<br>cylinder<br>sphere | Xenon-various shapes | 60 | 60<br>73<br>88 | This study |

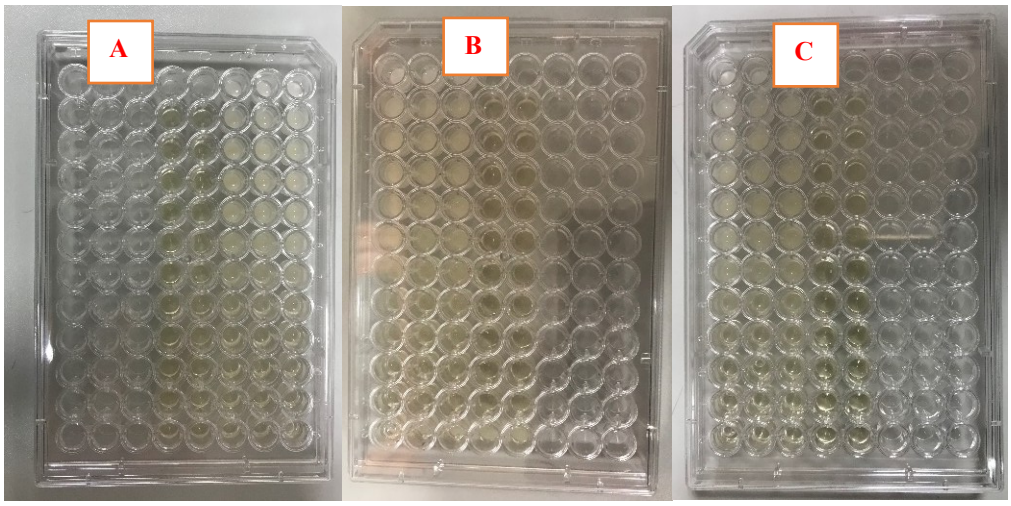


**Figure 10**. 96-well microplates for the antibacterial analysis

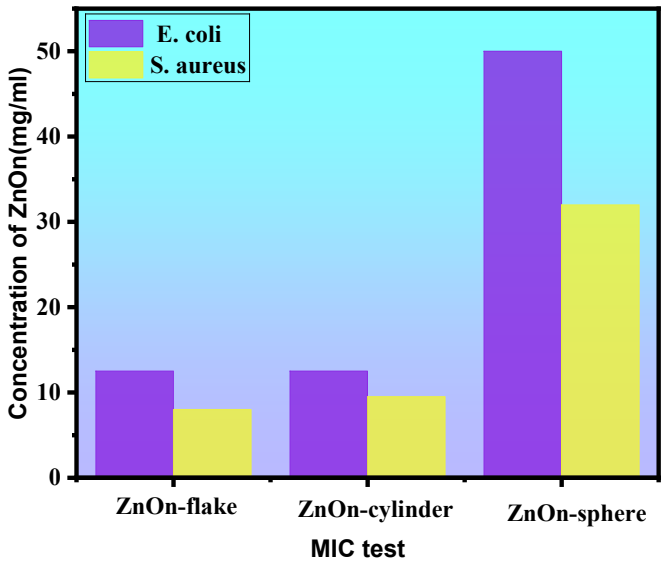


**Figure 11**. The MIC test for three ZnOn via fig leaf extract in different nanoparticle forms: A)flake, B)cylinder, C) sphere

**Table 2**. the comparative findings concerning ZnOn derived from various synthesis methods or extracts

| Method | Botanical extract | Type of test | Types of bacteria | Nanoparticles shape | Particle size(nm) | Efficiency | Ref |
|---|---|---|---|---|---|---|---|
| Green | *Calendula officinalis leaf* | disc diffusion | *S.aureus*<br>*K.pneumonia*<br>*E. coli.* | spherical | 28.23 | 35.2 ± 0.9<br>23.6 ± 0.1<br>13.5 ± 0.1(mm) | [93] |
| hydrothermal | ------ | disc diffusion | *S.aureus* | nanofiber | 51.35 | 16 (mm) | [94] |
| Green | *Cymbopogon citratus* | MIC | *E. coli*<br>*S.aureus* | rod-like | 20-24 | 92.07 ±0.13<br>88.13±0.35µg/ml | [95] |
| Green | *Viscum album leaf* | disc diffusion | *S.aureus* | quasi-spherical | 13.5 | 40±0.3 ( mm) | [96] |
| Co-precipitation | ----- | MIC | *S.aureus* | Spherical | 35 | 4 mg/ml | [97] |
| Green | *Equisetum diffusum D* | MIC | *L. monocytogenes*<br>*E. coli*<br>*B. bronchiseptica*<br>*S. epidermidis* | spherical | 57.94 ±1.8 | 30<br>70<br>90<br>20 | [69] |
| Green | *Ulva fasciata* | MIC | *S.aureus* | Flower & sphere | 77.81 | 22.5 µg/ml | [98] |

10.57647/ijc.2026.1601.10

Initially, 100 µL of Mueller-Hinton Broth was dispensed into a 96-well microplate. Subsequently, various concentrations of the submitted sample, ranging from 0.02 to 50 mg/ml, were established in the wells through a serial dilution technique. Finally, 100 microliters of bacterial suspension with a concentration of $10^6$ was added to the wells. To further validate the accuracy of the test, both negative control wells (comprising culture medium and solvent) and positive control wells (consisting of culture medium, solvent, and bacteria) were incorporated into the experimental design. Then the plates were incubated at 37 °C for 24 hours. Following this interval, the wells were assessed for the presence or absence of bacterial growth. The minimum concentration of the substance that effectively suppressed the development of the microorganism was identified as the MIC concentration. The Minimum Inhibitory Concentration (MIC) method results for (E. coli) the three samples ZnOn-flake, ZnOn-cylinder, and ZnOn-sphere are noted as 12.5, 12.5, and 50 mg/ml, and for (S. aureus) are determined as 8, 9.5, and 32 mg/ml, respectively. By minimizing nanoparticle size and increasing their surface area relative to volume, the antibacterial properties were enhanced, a finding corroborated by other research [89]. This study indicates that cylinder-shaped and nanoflake nanoparticles exhibit the highest antibacterial properties. In contrast, spherical nanoparticles demonstrate the least effect, a finding consistent with other research observations [90]. Furthermore, the antibacterial activity of ZnOn is generally stronger against S.aureus (Gram-positive) than E.coli (Gram-negative), which may be due to differences in cell wall structure and sensitivity to reactive oxygen species (ROS). This result has been proven by another research [91]. Because S.aureus (gram-positive) has a thick peptidoglycan layer but lacks a protective outer membrane, while E. coli (gram-negative) has an outer membrane rich in lipopolysaccharides (LPS) that acts as a barrier and reduces the penetration of ZnOn and reactive oxygen species (ROS) [92]. Figure 11 shows the approach used in the MIC analysis for three different samples against two types of bacteria. Additionally, Table 2 presents the comparative findings concerning ZnOn derived from various synthesis methods or extracts.

## 4. Conclusion

For the first time, this study synthesizes three different shapes of ZnOn with the same co-precipitation method, only with changing calcination temperatures (200 °C, 400 °C, and 600 °C). The impact of shapes is evaluated on characterization, photocatalyst, and anti-microbial activity. Because the shape plays a vital role in the applications of nanoparticles. Moreover, the findings of this study indicate that fig leaf extract represents a cost-effective, swift, non-toxic, and readily available approach for the synthesis of nanoparticles. The biomolecules in the fig leaf extract are crucial for the capping and stabilization processes involved in synthesizing ZnOn. The extract derived from fig leaves has been employed in producing ZnOn, which was subsequently produced in three nanoparticle shapes: flake, cylinder, and sphere. Besides exploring the photocatalytic activity associated with methylene orange (MO) degradation, the antibacterial capabilities of all three samples concerning *E.coli* and *S.aureus* were investigated. The reported efficiencies of photocatalytic activity for ZnOn in varying shapes of flake, cylinder, and sphere are 63.83%, 63.1%, and 53.39%, respectively. Results demonstrate that the sharper surface of nanoparticles increases photocatalyst activity. Various methods of characterization have been applied to analyze the optical and structural attributes of ZnOn, among which X-ray diffraction (XRD), field emission scanning electron microscopy (FESEM), Fourier-transform infrared spectroscopy (FTIR), and energy-dispersive X-ray spectroscopy (EDS) are particularly noteworthy. The findings on reactive oxygen species (ROS) production obtained from Energy Dispersive Spectroscopy (EDS) demonstrated the weight percentages of Zinc and Oxygen in three distinct ‘shapes’ of ZnOn. MIC test showed anti-microbial activity against Gram-negative (E. coli) and Gram-positive (S. aureus) bacteria for three ZnOn samples. The findings showed that the morphology of nanoparticles has a significant relationship with the production of reactive oxygen species (ROS), which affects their antibacterial activity. As the size of nanoparticles decreases, the increased surface area resulting in the production of reactive oxygen species also increases. In addition, this research demonstrated that green ZnOn may serve as an appropriate option for nanostructures (including nanocomposites, doping, etc.) and enhance efficiency in photocatalysis and anti-microbial applications. The ZnOn is effective against *s. aureus* bacteria owing to its cell wall, so they can be destroyed easily.

**Competing Interests**
The authors declare no competing interests.

**Ethics approval**
Not applicable

**Conflict of Interests**
The authors declare that they have no known competing financial interests or personal relationships that could have appeared to influence the work reported in this paper. No conflict of interest exists.

**Funding**
None

## References


[1] V. Despotović, N. Finčur, S. Bognar, D. Šojić Merkulov, P. Putnik, B. Abramović, and S. Panić, Separations. **10** (2023) 258. https://doi.org/10.3390/separations10040258

[2] M. P. Monopoli, C. Aberg, A. Salvati, K. A. Dawson, J. Biomed. Nanotechnol. (2020) 205-229. https://doi.org/10.1201/9780429399039

[3] Q. Saquib, M. Faisal, A. A. Al-Khedhairy, A. A. Alatar, Green synthesis of nanoparticles: Applications and prospects, First ed, Springer, 2020. https://doi.org/10.1007/978-981-15-5179-6

[4] M. Hamza, S. Muhammad, S. Zahoor, Acta Sci Appl. Phys. **2** (2022) 3-10.

[5] M. F. Ramadan, Fig (Ficus carica): Production, processing, and properties. First ed, Springer Nature, 2023 https://doi.org/10.1007/978-3-031-16493-4

[6] A. A. Barzinjy, S. M. Hamad, S. Aydın, M. H. Ahmed, F. H. Hussain, J. Mater. Sci.: Mater. Electron. **31** (2020) 11303. https://doi.org/10.1007/S10854-020-03679-Y

[7] N. Bala, S. Saha, M. Chakraborty, M. Maiti, S. Das, R. Basu, and P. Nandy, RSC Adv. **5** (2015) 4993. https://doi.org/10.1039/c4ra12784f

[8] D Saravanakkumar, S Sivaranjani, K Kaviyarasu, A. Ayeshamariam, B. Ravikumar, S. Pandiarajan, C. Veeralakshmi, M. Jayachandran, and M. Maaza. J. Semicond. **39** (2018) 033001. http://dx.doi.org/10.1088/1674-4926/39/3/033001

[9] T. U. D. Thi, T. T. Nguyen, Y. D. Thi, K. H. T. Thi, B. T. Phan, K. N. Pham, RSC Adv. **10** (2020) 23899. https://doi.org/10.1039/d0ra04926c

[10] S. Khoso, S. Mehar, I. Anam, N. Naheed, F. Saeed, N. Khan, and B. H. Abbasi, JAPS: J. Anim. Plant. Sci. **32** (2022) 229-237. https://doi.org/10.36899/JAPS.2022.1.0418

[11] J. Ghosh, N. S. Rupanty, T. Noor, T. R. Asif, T. Islam, V. Reukov, RSC Adv. **15** (2025) 10984. https://doi.org/10.1039/d5ra01429h

[12] R. Abbasi, G. Shineh, M. Mobaraki, S. Doughty, L. Tayebi, J. Nanoparticle Res. **25** (2023) 43. https://doi.org/10.1007/s11051-023-05690-w

[13] C. V. Restrepo, C. C. Villa, Environ. Nanotechnol., Monit. Manage. **15** (2021). 100428. https://doi.org/10.1016/j.enmm.2021.100428.

[14] S. Sharma, K. Kumar, N. Thakur, S. Chauhan, M. Chauhan, Bull. Mater. Sci. **43** (2020) 20. https://doi.org/10.1007/s12034-019-1986-y

[15] A. Mclaren, T. Valdes-Solis, G. Li, S. C. Tsang, J. Am. Chem. Soc. **131** (2009) 12540. https://doi.org/10.1021/ja9052703

[16] S. Salatin, S. Maleki Dizaj, A. Yari Khosroushahi, Cell Biol. Int. **39** (2015) 881. https://doi.org/10.1002/cbin.10459

[17] F. A-Z. Sayed, N. G. Eissa, Y. Shen, D. A. Hunstad, K. L. Wooley, M. Elsabahy, J. Nanobiotechnology. **20** (2022) 536. https://doi.org/10.1186/s12951-022-01733-x

[18] K. Öztürk, M. Kaplan, S. Çalış, Int. J. Pharm. **666** (2024) 124799. https://doi.org/10.1016/j.ijpharm.2024.124799

[19] Z. Nuri, M. S. Uddin, J. Curr. Res. Food Sci. **2** (2021) 07. https://www.doi.org/10.22271/foodsci

[20] M. F. Fazel, I. F. Abu, M. H. N. Mohamad, N. A. Mat Daud, A. N. Hasan, Z. Aboo Bakkar, M. A. N. Md Khir, N. Juliana, S. Das, M. R. Mohd Razali, and N. H. Zainal Baharin, Drug Des. Dev. Ther. **31** (2024) 1947-1968. https://doi.org/10.2147/DDDT.S436446

[21] M. F. Kurniawan, S. Apriliyanti, J Pharm Sci Community. **22** (2025) 30. https://doi.org/10.24071/jpsc.006449

[22] I. Fu. Rasool, A. Aziz, W. Khalid, H. Koraqi, S. A. Siddiqui, A. Al-Farga, W. F. Lai, and A. Ali, Molecules **28** (2023) 960. https://doi.org/10.3390/molecules28030960

[23] Y. I. ElAchaouia, J. Fakhfakh, M. Adhar, M. Affes, S. Tounsi, N. Allouche, Chem. Afr. **6** (2023) 1163. https://doi.org/10.1007/s42250-023-00600-y

[24] A. El. Ghouizi, D. Ousaaid, H. Laaroussi, M. Bakour, A. Aboulghazi, R. S. Soutien, C. Hano, and B. Lyoussi, Foods. **12** (2023) 759. https://doi.org/10.3390/foods12040759

[25] S. Mawa, K. Husain, I. Jantan, J. evid.-based complement. altern. med. **2013** (2013) 974256. https://doi.org/10.1155/2013/974256

[26] A. Dewi, F. Rahmayanti, H. Bagir, A. F. Jannah, A. Winanta, Online J. Biol. Sci. **23** (2023) 71. https://doi.org/10.3844/OJBSCI.2023.71.80

[27] M. Y. Al-darwesh, S. S. Ibrahim, L. L. Hamid, Nano-Struct. Nano-Objects. **38** (2024) 101163. https://doi.org/10.1016/j.nanoso.2024.101163

[28] F. F. Soleimani, T. Saleh, S. A. Shojaosadati, R. Poursalehi, Bionanoscience. **8** (2018) 72. https://doi.org/10.1007/s12668-017-0423-1

[29] S. Anjum, M. Hashim, S. A. Malik, M. Khan, J. M. Lorenzo, B. H. Abbasi, and C. Hano, Cancers. **13** (2021) 4570. https://doi.org/10.3390/cancers13184570

[30] S. Mustapha, M. Ndamitso, A. Abdulkareem, J. O. Tijani, D. T. Shuaib, A. K. Mohammed, and A. Sumaila, Adv. Nat. Sci.: Nanosci. **10** (2019) 045013. http://doi.org/10.1088/2043-6254/ab52f7

[31] M. T. Ulhakim, S. Sukarman, K. Khoirudin, N. Fazrin, T. Irfani, A. Hakim, Indones. J. Appl. Phys. **14** (2024) 141-150. https://doi.org/10.13057/ijap.v14i1.79195.

[32] V. Venu Gopal, S. Kamila, Appl. Nanosci. **7** (2017) 75. https://doi.org/10.1007/s13204-017-0553-3

[33] P. Mahmoodi, A. Motavalizadehkakhky, M. Darroudi, J. Mehrzad, R. Zhiani, Bioprocess Biosyst. Eng. **46** (2023) 1163. https://doi.org/10.1007/s00449-023-02888-z

[34] M. A. Irshad, M. Latif, I. Nasim, R. Nawaz, A. F. Zahoor, A. A. Al-Mutairi, S. A. Al-Hussain, A. Irfan, and M. E. Zaki, Ecotoxicol. Environ. Saf. **281** (2024) 116616. https://doi.org/10.1016/j.ecoenv.2024.116616

[35] N. Abbes, I. Bekri, M. Cheng, N. Sejri, M. CHEIKHROUHOU, X. Jun, Mater. Sci. **28** (2022) 144. https://doi.org/10.5755/j02.ms.28314

[36] N. Sedefoglu, Ceram. Int. **50** (2024) 9884. https://doi.org/10.1016/j.ceramint.2024.01.387

[37] P. Luque, C. Soto-Robles, O. Nava, C. M. Gomez-Gutierrez, A. Castro-Beltran, H. E. Garrafa-Galvez, A. R. Vilchis-Nestor, and A. Olivas, J. Mater. Sci.: Mater. Electron. **29** (2018) 9764. https://doi.org/10.1007/s10854-018-9015-2

[38] S. Pasieczna-Patkowska, M. Cichy, J. Flieger, Molecules. **30** (2025) 684. https://doi.org/10.3390/molecules30030684

[39] A. R. Mendes, C. M. Granadeiro, A. Leite, E. Pereira, P. Teixeira, F. Poças, J. Nanomater. **14** (2024) 638. https://doi.org/10.3390/nano14070638

[40] J. Osuntokun, D. C. Onwudiwe, E. E. Ebenso, Green Chem. Lett. Rev. **12** (2019) 444. https://doi.org/10.1080/17518253.2019.1687761

[41] U. Pachauri, D. P. Joshi, N. Arora, Appl. Phys. A. **126** (2020) 253. http://doi.org/10.1007/s00339-020-3411-1

[42] L. Umaralikhan, M. J. M. Jaffar, J. Mater. Sci.: Mater. Electron. **28** (2017) 7677. https://doi.org/0.1007/s10854-017-6461-1

[43] M. Singh, M. Goyal, K. Devlal, J. Taibah Univ. SCI. **12** (2018) 470. https://doi.org/10.1080/16583655.2018.1473946

[44] K. Baishya, J. S. Ray, P. Dutta, P. P. Das, S. K. Das, Appl. Phys. A. **124** (2018) 1. http://doi.org/10.1007/s00339-018-2097-0

[45] J. Klein, L. Kampermann, B. Mockenhaupt, M. Behrens, J. Strunk, G. Bacher, Adv. Funct. Mater. **33** (2023) 2304523. https://doi.org/10.1002/adfm.202304523

[46] B. J. Abdullah, Mater. Sci. Semicond. Process. **137** (2022) 106214. https://doi.org/10.1016/j.mssp.2021.106214

[47] N. Sedefoglu, Optik. **288** (2023) 171217. https://doi.org/10.1016/j.ijleo.2023.171217

[48] D. Zhou, A. A. Keller, Water Res. **44** (2010) 2948. https://doi.org/10.1016/j.watres.2010.02.025

[49] N. Torres-Gómez, O. Nava, L. Argueta-Figueroa, R. García-Contreras, A. Baeza-Barrera, A. R. Vilchis-Nestor, J. Nanomater. **2019** (2019) 7921273. https://doi.org/10.1155/2019/7921273

[50] R. Z. Moghadam, H. R. Dizagi, H. Agren, M. H. Ehsani, J. Sci. Rep. **13** (2023) 17556. https://doi.org/10.1038/s41598-023-44947-1

[51] C. Qi, S. Musetti, L-H. Fu, Y-J. Zhu, L. Huang, Chem. Soc. Rev. **48** (2019) 2698. https://doi.org/10.1039/C8CS00489G

[52] M. Jothibas, E. Paulson, A. Mathivanan, S. Srinivasan, K. S. Kannan, Nanotechnol. Environ. Eng. **8** (2023) 511. https://doi.org/10.1007/s41204-023-00310-3

[53] M. M. Ba-Abbad, A. Benamour, D. Ewis, A. W. Mohammad, E. Mahmoudi, Jom. **74** (2022) 3531. http://doi.org/10.1007/S11837-022-05380-3

[54] X. Wang, K. Maeda, A. Thomas, K. Takanabe, G. Xin, J. M. Carlsson, K. Domen, and M. Antonietti, Nat. Mater. **8** (2009) 76. https://doi.org/10.1038/nmat2317

[55] M. Naushad, S. Rajendran, E. Lichtfouse, Green photocatalysts. first ed, Springer, 2020. https://doi.org/10.1007/978-3-030-15608-4

[56] M. Rezaei, E. Heydari-Bafrooei, A. A. Ensafi, J. Alloys Compd. (2025) 181214. https://doi.org/10.1016/j.jallcom.2025.181214

[57] E. Heydari-Bafrooei, M. Sabet, Z. Alizadeh, R. Ghazanfarpour, M. H. Moazzen, M. Rezaei, S. S. Varnoosfaderani, and M. Ahmadi, Mater. Chem. Phys. **332** (2025) 130254. https://doi.org/10.1016/j.matchemphys.2024.130254

[58] M. Rezaei, A. A. Ensafi, E. Heydari-Bafrooei, J. Ind. Eng. Chem. **146** (2025) 589. https://doi.org/10.1016/j.jiec.2024.11.043

[59] M. Rezaei, A. A. Ensafi, Mater. Sci. Semicond. Process. **188** (2025) 109162. https://doi.org/10.1016/j.mssp.2024.109162.

[60] H. Ahmad, A. B. Siddique, S. Zaheer, R. Sattar, A. Abbas, M. Amin, R. Al-Salahi, H. A. Abuelizz, and M. Z. Saleem, J. Water Process Eng. **74** (2025) 107855s https://doi.org/10.1016/j.jwpe.2025.107855

[61] M. Rezaei, A. Nezamzadeh-Ejhieha, Int. J. Hydrogen Energy. **45** (2020) 24749. https://doi.org/10.1016/j.ijhydene.2020.06.258

[62] S. Ghaffar, A. Abbas, M. Naeem-ul-Hassan, N. Assad, M. Sher, S. Ullah, H. A. Alhazmi, A. Najmi, K. Zoghebi, M. Al Bratty, and A. Hanbashi, Antioxidants. **12** (2023) 1201. https://doi.org/10.3390/antiox12061201

[63] S. Cao, J. Jiang, B. Zhu, J. Yu, Phys. Chem. Chem. Phys. **18** (2016) 19457. https://doi.org/10.1039/C6CP02832B

[64] Y-F. Li, Z-P. Liu, J. Am. Chem. Soc. **133** (2011) 15743. https://doi.org/10.1021/ja206153v.

[65] A. Abbas, S. Mansoor, M. H. Nawaz, A. A. Chaudhry, K. Ijaz, S. Riaz, and A. Hayat, RSC Adv. **13** (2023) 11537. https://doi.org/10.1039/D3RA01268A

[66] A. Zheng, C. Abdullah, E. Chung, Y. Andou, Int. J. Environ. Sci. Technol. **20** (2023) 5753. http://doi.org/10.1007/s13762-022-04354-x

[67] W. Yu, J. Zhang, T. Peng, Appl. Catal., B. **181** (2016) 220. https://doi.org/10.1016/j.apcatb.2015.07.031

[68] L. A. Wali, A. M. Alwan, A. B. Dheyab, D. A. Hashim, Optik. **179** (2019) 708. https://doi.org/10.1016/j.ijleo.2018.11.011

[69] N. Assad, A. Abbas, M. F. ur Rehman, M. Naeem-ul-Hassan, RSC adv. **14** (2024) 22344. https://doi.org/10.1039/D4RA03573A

[70] A. B. Siddique, M. A. Shaheen, A. Abbas, Y. Zaman, M. A. Bratty, A. Najmi, A. Hanbashi, M. Mustaqeem, H. A. Alhazmi, Z. ur Rehman, and K. Zoghebi, Heliyon. **10** (2024). http://doi.org/S2405-8440(24)16710-2

[71] B. Akram, K. Ahmad, J. Khan, B. A. Khan, J. Akhtar, New J Chem. **42** (2018) 10947. https://doi.org/10.1039/C8NJ02317D

[72] S. Rajendran, M. Naushad, L. C. Ponce, E. Lichtfouse, Green photocatalysts for energy and environmental process. First ed, Springer, 2020. https://doi.org/10.1007/978-3-030-17638-9

[73] A. Rani, R. Reddy, U. Sharma, P. Mukherjee, P. Mishra, A. Kuila, L. C. Sim, and P. Saravanan, J. Nanostructure Chem. **8** (2018) 255. http://doi.org/10.1007/S40097-018-0278-1

[74] Y. C. Liu, J. Li, J. Ahn, J. Pu, E. J. Rupa, Y. Huo, and D. C. Yang, Optik. **218** (2020) 165245. https://doi.org/10.1016/j.ijleo.2020.165245

[75] Y. Zheng, L. Fu, F. Han, A. Wang, W. Cai, J. Yu, J. Yang, and F. Peng, Green Chem. Lett. Rev. **8** (2015) 59. https://doi.org/10.1080/17518253.2015.1075069

[76] P. Nethravathi, G. Shruthi, D. Suresh, H. Nagabhushana, S. Sharma, Ceram. Int. **41** (2015) 8680. https://doi.org/10.1016/j.ceramint.2015.03.084

[77] A. Ekennia, D. Uduagwu, O. Olowu, O. Nwanji, O. Oje, B. Daniel, S. Mgbii, and C. Emma-Uba, Micron. **141** (2021) 102964. https://doi.org/10.1016/j.micron.2020.102964

[78] M. Uribe-López, M. Hidalgo-López, R. López-González, D. M. Frías-Márquez, G. Núñez-Nogueira, D. Hernández-Castillo, and M. A. Alvarez-Lemus, J. Photochem. Photobiol. A: Chem. **404** (2021) 112866. https://doi.org/10.1016/j.jphotochem.2020.112866

[79] A. Bhosale, K. Abitkar, P. Sadalage, K. Pawar, K. Garadkar, J. Mater. Sci.: Mater. Electron. **32** (2021) 20510. https://doi.org/10.1007/s10854-021-06563-5

[80] S. Ullah, M. Shaban, A. B. Siddique, A. Zulfiqar, N. S. Lali, M. Naeem-ul-Hassan, M. I. Irfan, M. Sher, M. F. ur Rehman, A. Hanbashi, and F. Y. Sabei, J. Environ. Chem. Eng. **12** (2024) 113350. https://doi.org/10.1016/j.jece.2024.113350

[81] Q. Gao, Z. Feng, J. Wang, F. Zhao, C. Li, J. Ju, Crit. Rev. Food Sci. **65** (2025) 4327. https://doi.org/10.1080/10408398.2024.2387327

[82] C. R. Mendes, G. Dilarri, C. F. Forsan, V. D. M. R. Sapata, P. R. M. Lopes, P. B. de Moraes, R. N. Montagnolli, H. Ferreira, and E. D. Bidoia, J. Sci. Rep. **12** (2022) 2658. https://doi.org/10.1038/s41598-022-06657-y

[83] V. Lakshmi Prasanna, R. Vijayaraghavan, Langmuir. **31** (2015) 9155. https://doi.org/10.1021/acs.langmuir.5b02266

[84] L-E. Shi, Z-H. Li, W. Zheng, Y-F. Zhao, Y-F. Jin, Z-X. Tang, Food Addit. Contam. **31** (2014) 173. https://doi.org/10.1080/19440049.2013.865147

[85] I. Ul Haq, R. Pinto Vieira, W. G. Lima, M. E. de Lima, K. Krukiewicz, Arab j. basic appl. sci. **31** (2024) 325. https://doi.org/10.1080/25765299.2024.2366543

[86] F. S. Mustafa, A. A. Oladipo, J. Water Process Eng. **42** (2021) 102132. https://doi.org/10.1016/j.jwpe.2021.102132

[87] A. Biswas, U. Kar, N. R. Jana, Phys. Chem. Chem. Phys. **24** (2022) 13965. https://doi.org/10.1039/D2CP00301E

[88] NaH. Alshraiedeh, O. F. Ammar, M. M. Masadeh, K. H. Alzoubi, M. G. Al-Fandi, R. J. Oweis, R. H. Alsharedeh, R. A. Alabed, and R. H. Hayajneh, Curr. Nanosci. **18** (2022) 758. https://doi.org/10.2174/1573413718666220303153123

[89] S. Sharma, K. Kumar, N. Thakur, S. Chauhan, M. Chauhan, Bull. Mater. Sci. **43** (2020) 1. https://doi.org/10.1007/s12034-019-1986-y

[90] F. Y. Rezaei, G. Pircheraghi, V. S. Nikbin, ACS Appl. Nano Mater. **7** (2024) 15242. https://doi.org/10.1021/acsanm.4c02046

[91] B. Akram, K. Ahmad, J. Khan, B. A. Khan, J. Akhtar, New J Chem. **42** (2018) 10947. https://doi.org/10.1039/C8NJ02317D

[92] H. Samadi, R. Z. .Mohgadam, and M. G. Shahraki, Green synthesis of ZnO nanoparticles, photocatalyst activity and its biomedical applications: A review. Mater. Chem. Phys. **345** (2025). 131161. https://doi.org/10.1016/j.matchemphys.2025.131161

[93] A. K. Tiwari, S. Jha, S. K. Tripathi, R. Shukla, R. R. Awasthi, A. K. Bhardwaj, A. K. Singh, and A. Dikshit, Discov. appl. sci. **6** (2024) 399. https://doi.org/10.1007/s42452-024-06049-z

[94] M. R. Khaleel, F. S. Hashim, A. H. O. Alkhayatt, Ceram. Int. **50** (2024) 40161. https://doi.org/10.1016/j.ceramint.2024.07.283

[95] Y. H. I. Mohammed, S. Alghamdi, B. Jabbar, D. Marghani, S. Beigh, A. S. Abouzied, N. E. Khalifa, W. M. Khojali, B. Huwaimel, D. H. M. Alkhalifah, and W. N. Hozzein, ACS omega. **8** (2023) 32027. https://doi.org/10.1021/acsomega.3c03908

[96] W. Mushtaq, M. Ishtiaq, M. Maqbool, M. W. Mazhar, R. Casini, A. M. Abd-ElGawad, and H. O. Elansary, Plants. **12** (2023) 2130. https://doi.org/10.3390/plants12112130

[97] D. Manyasree, P. Kiranmayi, R. K. Venkata, Int J App Pharm. **10** (2018) 224. http://dx.doi.org/10.22159/ijap.2018v10i6.29376

[98] M. S. Alsaggaf, A. M. Diab, B. E. ElSaied, A. A. Tayel, S. H. Moussa, J. Nanomater. **11** (2021) 385. https://doi.org/10.3390/nano11020385

10.57647/ijc.2026.1601.10